C Journal of Carbon Research

MDPI

Review

Porphyrin MOF-Derived Porous Carbons: Preparation and Applications

Flávio Figueira * and Filipe A. Almeida Paz

Department of Chemistry, CICECO-Aveiro Institute of Materials, University of Aveiro, 3810-193 Aveiro, Portugal; filipe.paz@ua.pt

* Correspondence: ffigueira@ua.pt

Abstract: Metal–organic frameworks (MOFs) are crystalline materials with permanent porosity, composed of metal nodes and organic linkers whose well-ordered arrangement enables them to act as ideal templates to produce materials with a uniform distribution of heteroatom and metal elements. The hybrid nature of MOFs, well-defined pore structure, large surface area and tunable chemical composition of their precursors, led to the preparation of various MOF-derived porous carbons with controlled structures and compositions bearing some of the unique structural properties of the parent networks. In this regard, an important class of MOFs constructed with porphyrin ligands were described, playing significant roles in the metal distribution within the porous carbon material. The most striking early achievements using porphyrin-based MOF porous carbons are here summarized, including preparation methods and their transformation into materials for electrochemical reactions.

Keywords: metal–organic frameworks; porous carbons; porphyrins; electrochemistry

Citation: Figueira, F.; Paz, F.A.A. Porphyrin MOF-Derived Porous Carbons: Preparation and Applications. *C* **2021**, *7*, 47. https://doi.org/10.3390/c7020047

Academic Editor: Jean-François Morin

Received: 16 April 2021
Accepted: 12 May 2021
Published: 15 May 2021

1. Introduction

Metal–organic frameworks (MOFs) are hybrid materials formed by organic ligands and metal ions/clusters exhibiting, as a whole, remarkable properties which include large internal surface areas, porosity, unsaturated and accessible metal sites, functional diversity, and adjustable structure and compositions [1,2]. They have been extensively studied over the last two decades in a wide range of applications that include adsorption, gas storage, catalysis, drug release, biomedical applications, biosensing and, more recently, food safety [3–8].

The electrochemical applications of MOFs did not experience the same level of growth in research over the years, mainly because these compounds are, in general, insulators or semiconductors with diminished electrolyte ion transport capabilities [9]. The intrinsic surface area, adsorption ability and chemical stability can dramatically decrease for some MOFs when exposed to moisture, ultimately hampering their performance [10]. A bolder but efficient strategy to increase the electrochemical performance of MOFs is to mix them with conductive materials (e.g., metal nanocrystals, carbon nanostructures, conductive polymers, among others), or take advantage of their porosity to favor the inclusion of non-native conductivity by infusing the accessible pore volume with conductive guest molecules [11–13]. Other strategies were developed to overcome the insufficiencies of MOFs, particularly the usage of core–shell architectures, morphological control at the nanoscale and conversion to hollow structures [14–16].

Chemical tuning of the functional linkers may lead to a better charge transfer inside the framework itself [17,18]. The incorporation of redox-active organic ligands (benzene, pyridine, imidazole, and thiophene) takes advantage of their conjugated system, ultimately facilitating UV absorption, luminescent emission, and charge mobility [19,20]. This is particularly important when porphyrins are the selected functional ligands [21].

Metalloporphyrins exist in many biological systems with various functions, including light-harvesting, oxygen transport, and catalytic systems. Many non-natural porphyrin

systems are used in supramolecular chemistry, biomedical applications (photodynamic therapy), photodynamic inactivation, catalysis, and photocatalysis [22–28]. With various coordinating moieties rationally included in peripheral positions, the stable and rigid structures of porphyrins are excellent candidates to act as primary building blocks in the construction of electroactive MOFs [29–31]. Additionally, porphyrins allow decoration of the inner pores of the MOFs with coordinatively unsaturated metal centers (i.e., open metal sites), greatly enriching their electrochemical properties and applications [32]. A wide range of porphyrin-based MOFs have been prepared throughout the years with diverse structures and intriguing properties, which can be applied in hydrogen storage, molecular sorption, sensing, photonics, and heterogeneous catalysis [33–39].

Even though a large number of these MOFs have limited charge conduction pathways, and new techniques are currently being developed to form uniform MOF films with improved interfacial contact [40], new design strategies based on transforming MOFs into more conductive materials such as porous carbons (PCs) will likely emerge in the coming years to fill a niche in electronic applications where enhanced flexibility and high charge mobility are priorities.

Porphyrin-Based MOF Porous Carbons

Compared with other carbons such as activated carbons, carbon nanotubes (CNTs), and graphene, MOF-derived PCs provide an easy way for pore and shape control and heteroatom loading by carefully selecting the MOF linkers and the carbonization conditions [41]. This is particularly important because the PCs support an extended surface area and hierarchical pores that guarantee free diffusion of substrates [42]. In addition, the high degree level of graphitized carbon significantly enhances electrical conductivity as well as chemical and thermal stabilities [43].

Noteworthy, the production cost of MOF-derived carbons is higher than those of carbons obtained by conventional methods. The controllable particle sizes and shapes of the carbons obtained via pyrolysis of porphyrin-based MOFs can, by far, compensate for the aspects involving production cost and environmental friendliness. Furthermore, several porphyrin-based MOFs can be obtained by sustainable methodologies, revamping the PC process from MOFs if the merits of the materials outperform those of the parent precursors [44].

In general, the preparation of MOF-derived PCs consists mainly of two procedures in which PC catalysts derived from MOFs must undergo high-temperature pyrolysis. One uses the MOF as a sacrificial template that incorporates additional carbon sources inside the pores. In this case, several organic compounds can impregnate the pore space and subsequent carbonization generates the PC with additional elements. This is particularly interesting when a high degree of nitrogen (or other element content) is required to improve the degree of graphitization to further increase the conductivity of the PC. Another method to prepare PCs is through direct carbonization of the MOF having empty pores because it contains abundant organic species that can be used as carbon precursors. Both methods have numerous advantages to prepare carbons with desirable nanostructures and functions, however, the direct carbonization approach is clearly the most common (Figure 1).

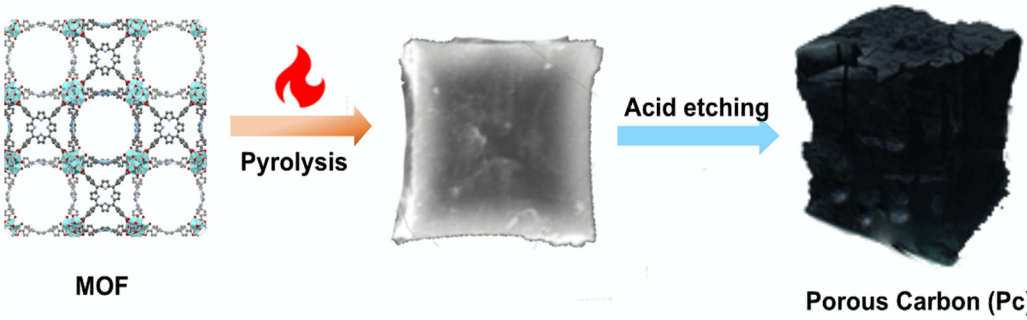

Figure 1. Schematic illustration of the procedure used to prepare a PC from MOFs as sacrificial templates. Color scheme: Zr (**light blue**); O (**red**); N (**blue**); C (**grey**).

The MOF-derived PC inherits some of the characteristics of the parent MOFs by adjusting the synthesis process (e.g., by varying the gas atmosphere, annealing process and the precursor amount). The use of porphyrin-based MOFs is advantageous when PC-rich heteroatom or metal elements are required for fine-tuning the applicability of the final material [42]. Several porphyrin-based MOFs reported in the literature have been used towards this end, with the most widely employed being the so-called porous coordination networks (PCNs). Figure 2 illustrates some of the most iconic structures used and described in this review [45].

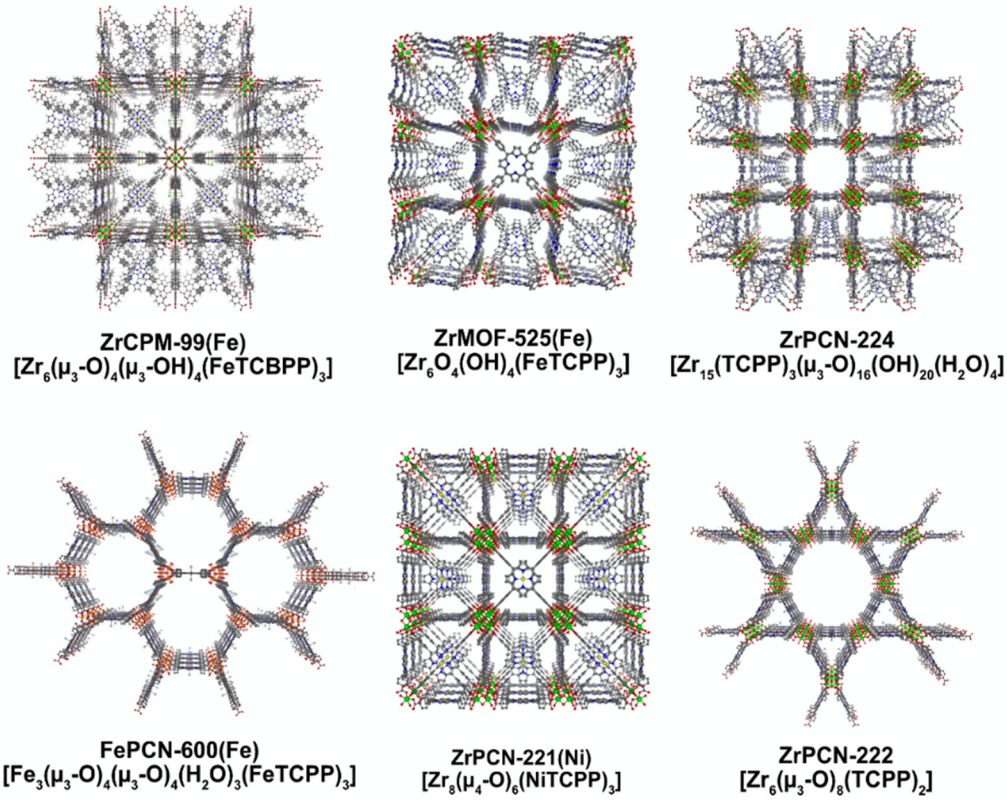

Figure 2. Porphyrin-based MOFs that can be transformed into PC functional materials. Color scheme: Zr (green); Fe (orange); Ni (yellow) O (red); N (blue); C (grey).

This review focuses on the PCs obtained from porphyrin-based MOFs pyrolysis, with most of these materials being developed as electrocatalysts. The following discussion is mainly focused on the structural properties and features of the final PC materials, though applications are addressed when pertinent.

2. Porous Carbons from Porphyrin-Based MOFs

One of the driving forces towards the development of MOF-derived PC materials is associated with the homogeneous distribution of nitrogen atoms. The periodic arrangement of different atoms in highly ordered MOF structures offers congenital conditions for homogeneous atomic distribution. Therefore, MOFs based on nitrogen-containing organic ligands, such as porphyrins, would enable the resultant nitrogen atoms to be well distributed throughout the PC matrix upon pyrolysis. Furthermore, special attention is devoted to these systems based on the concept that porphyrin-based MOFs provide the opportunity to prepare M–N–C catalysts that, after pyrolysis, give rise to materials with active and stable M–N_x moieties (the M–N_x denominations indicate M is a 4th-period *d*-transition metal (e.g., Fe, Co, Mn), and *x* indicates the number of N atoms coordinated to the metal) [46,47]. This has implications in the catalytic effect of several electrocatalytic reactions and on the stability of the PC catalyst itself [29].

2.1. Metal-Free Mof-Derived PC

Only a handful of reports describe metal-free porphyrin MOF-based PCs [48–50]. These materials, however, are of great importance and can be envisaged as alternative candidates to conventional metal-based catalysts in many reactions. One striking example was reported by Huang et al. with the pyrolysis at 700 °C of ZrPCN-224 [48]. The PC carbon obtained after acid etching comprises amorphous carbon coated with well-defined graphene layers, offering a high surface area (1089 m^2g^{-1}), hierarchical pores, and high nitrogen content (3.08 wt%, mainly pyrrolic nitrogen species, Figure 3A). Remarkably, as a metal-free catalyst, ZrPCN-224/PC exhibited excellent activity in the catalytic reduction of 4-nitrophenol to 4-aminophenol in the presence of $NaBH_4$ under ambient conditions (pseudo-first-order kinetics and the reaction rate constant was up to $k = 5.3 \times 10^{-3}$ s^{-1}).

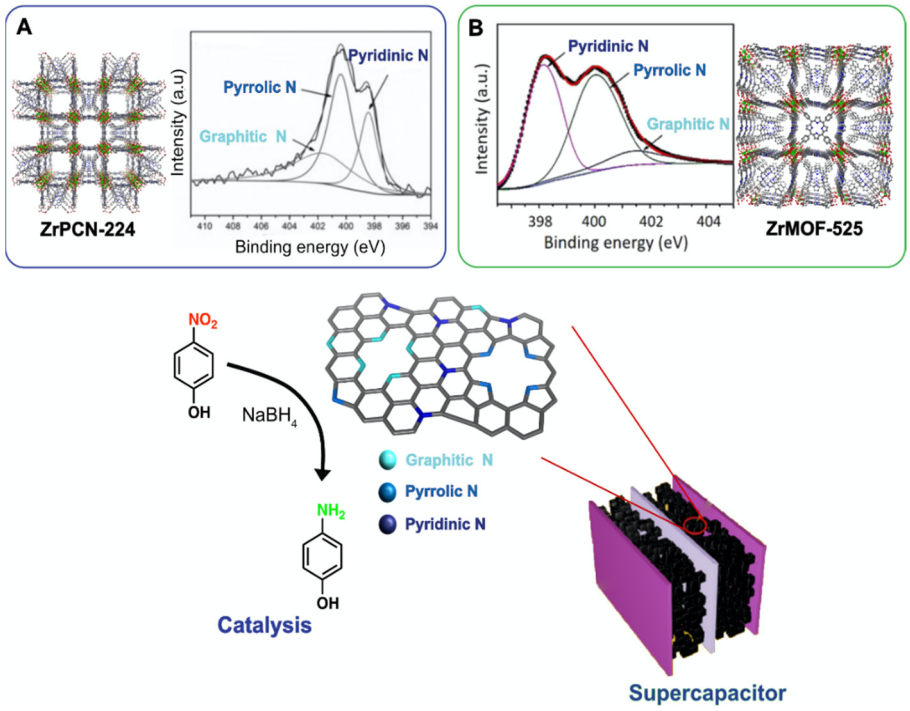

Figure 3. Schematic representation of applications where PC prepared with ZrPCN-224 and ZrMOF-525 are used. (**A**) Structure of ZrPCN-224 and XPS spectra of the porous carbon. (**B**) Structure of ZrMOF-525 and XPS spectra of the porous carbon. Reproduced with permission from [48,49]. Wiley-VCH, 2016 and 2017.

In an attempt to prepare novel supercapacitor materials, it was not by accident that porphyrin-based MOF derived PCs found their way into this application. In 2017, a MOF-

525-derived PC was prepared reporting specific capacitance values (425, 361, 347, 312, and 244 $F \cdot g^{-1}$) measured at various current densities (2, 4, 5, 7, and 10 $A \cdot g^{-1}$) [49]. The authors attributed the specific capacitance observed for this PC to nitrogen- and oxygen-containing functional groups (carbon 88.3% is present with trace amounts of nitrogen 6.7% and oxygen 5.0%), improving surface wettability (Figure 3B).

Throughout these studies, the morphology of the initial MOFs has the tendency to be inherited by the PC materials. This was elucidated by Hou et al. when studying the relationship between the pore structures between the MOF precursors and the corresponding derived carbon materials [50]. They noticed that ZrPCN-222- and ZrPCN-224-derived PCs showed shallow BET surface areas and confirmed, by SEM and TEM, that carbonized products from ZrPCN-222 and ZrPCN-224 at two different temperatures (1000 and 800 °C), aside from a small shrinkage behavior, inherited the rod and cubic morphologies from the parent MOFs (Figure 4).

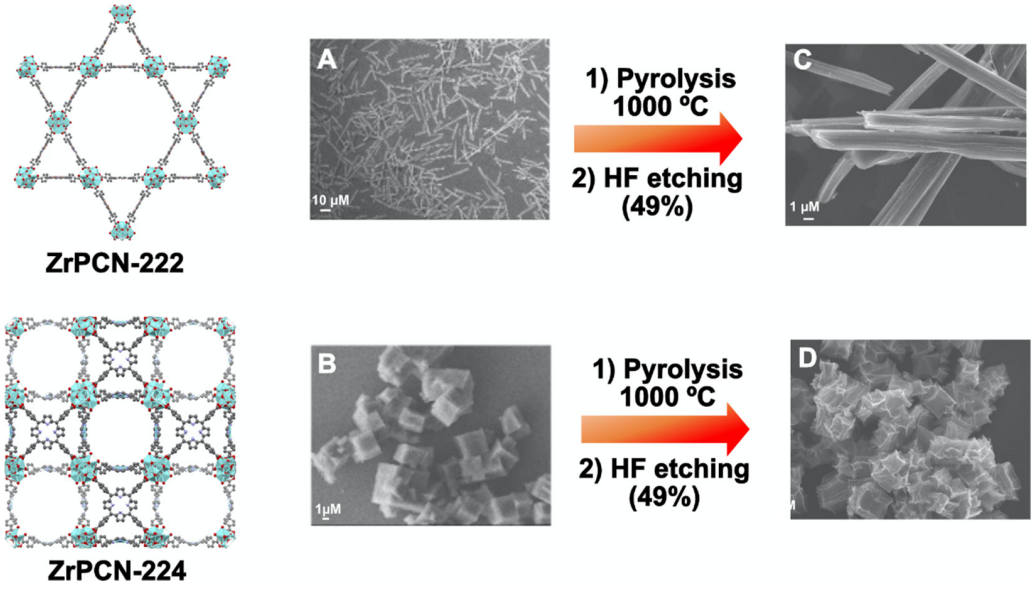

Figure 4. Schematic illustration for the pyrolysis treatment performed on ZrPCN222 and ZrPCN224. SEM images of: (**A**) ZrPCN-222; (**B**) PCN-224; (**C**) ZrPCN-222/PC; and (**D**) ZrPCN-224/PC. Color scheme: Zr (light blue); O (red); N (blue); C (grey). Reproduced with permission from [50]. Elsevier, 2020.

Both these materials showed a positive onset potential and high current density for carbon dioxide reduction reactions (CO_2RR), which was attributed to the large BET surface areas and accessible exposed active sites to CO_2. Pyrolysis of ZrPCN-224/PC under an NH_3 flow at 1000 °C for 0.5 h increased the selectivity at a lower potential (−0.9 to −1.0 V vs. RHE), and the highest FE of CO maintained 60% when the potential was −0.9 V (vs. RHE). The major reason for this practical difference resides in the higher amount of pyrrolic nitrogen (49.5%) in ZrPCN-224NH_3/PC, while the content of the pyridinic nitrogen and graphitic nitrogen decreased.

2.2. Metal MOF-Derived PC Materials

Transition metal–nitrogen–carbon (M–N–C, M = Fe, Co, Ni and Cu) materials with porphyrins are promising candidates for electrocatalysts because of their high activity and excellent stability. The success of these materials resides on the active M–N_x–C (M = Fe, Co, Ni and Cu) site with the M–N_4 coordination environment being similar to that of the biological heme unit for O_2 activation and reduction processes. Because of the well-ordered structures of these compounds, the chemical and catalytic features of the M–N_4 active sites can be regulated by tuning the parent structures into PC materials.

An excellent example of the precision obtained by these structures was demonstrated with the preparation of a series of non-interpenetrated MOFs (CPM-99) with the extended tetrakis (4-carboxybiphenyl) porphyrin (BPP) (Figure 5) [51].

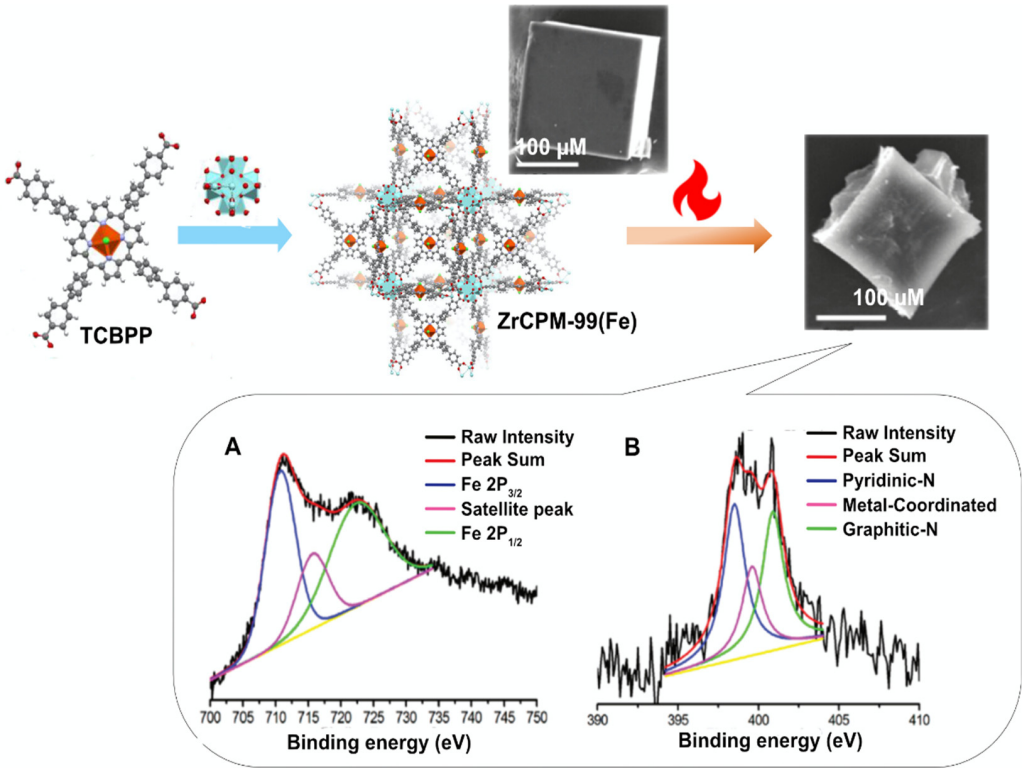

Figure 5. Schematic preparation of a porous carbon from ZrCPM-99 (Fe) with SEM images for the parent ZrCPM-99 (Fe) MOF and the material obtained from pyrolysis. A 3D network with Zr6 clusters depicted as polyhedra. Color scheme: Zr (light blue); Fe (orange); O (red); N (blue); C (grey). (**A**,**B**) XPS Fe 2p and N 1s spectra of the ZrCPM-99 (Fe) PC. Reproduced with permission from [51]. American Chemical Society, 2015.

The highly porous and stable nature of the ZrCPM-99 (Fe) network with iron porphyrin-based pore walls proved to be well suited as a precursor, without additional metal species or nitrogen/carbon sources, to prepare PC materials. After the carbonization process at 700 °C, the iron PC material exhibited high oxygen-reduction reaction (ORR) activity (with an onset potential of 0.95 and 0.88 V in alkaline and acidic electrolytes, respectively), comparable to a 20% Pt/C catalyst (0.978 and 0.880 V, respectively). The efficient electrocatalytic activity of ZrCPM-99 (Fe)/PC was attributed to its unique large cavity with a heme-like center topology. This work demonstrated that the rational topological design of porphyrin-based porous MOFs could be an effective strategy to achieve high performance in electrocatalysis. We note that the cubic crystal morphology and the porous nature of the parent MOF network was retained after pyrolysis.

Another example of the usage of bulk MOF single crystals to achieve useful ORR PC materials concerns the pyrolysis of ZrPCN-222 (Cu) at 900 °C in the presence of small amounts of air [52]. The results suggest that samples treated with air show a significant increase in surface areas and a better electron transfer, indicating that a partial etching of the carbon in these conditions increases the porosity and accessibility to highly active catalytic sites.

Changing the transition metal dopants to noble metals such as rhodium, iridium or platinum, and the metallic nodes to hafnium, HfPCN-222, it was possible to produce by pyrolysis noble metal PC materials capable of being used in hydrogen evolution reactions (HER) [53]. In this regard, the PC obtained by the carbonization of HfPCN-222 (Ir) at

700 °C displays an onset potential of 0.011 V, a low overpotential of 0.032 V at a current density of 10 mA·cm^{-2} (HER performances of the prepared HfPCN-222 (Ir) are studied by steady-state linear sweep voltammetry (LSV) in a 0.5 M H_2SO_4 solution (pH = 0.36). For comparison, the onset potential and overpotential at a current density of 10 mA·cm^{-2} of the commercial 20% Pt/C are 0.014 and 0.033 V, respectively.

Other examples using direct carbonization processes on porphyrin-based MOFs tend to promote structural collapse, resulting in bulk carbons with limited access to the catalytic sites. Nonetheless, a handful of methodologies have been modified to address these limitations. For instance, Hua et al. developed a NaCl salt-assisted pyrolytic approach to prevent small crystal aggregation at high temperatures, allowing crystal morphological transference to the final PC materials [54]. Optimization of the post-activation procedure with concentrated sulfuric acid worked in synergy with NaCl to prevent over-etching the final PC materials. This complete process produced a PC structure with efficient accessibility of the active sites (with an onset potential for ORR of 1.01 and 0.94 V in alkaline and acidic electrolytes, respectively (V vs. RHE)), a high graphitization level, and good electrolyte stability and durability. Another methodology to control the morphology of PC materials is possible with a systematic carbonization temperature control. Recently, Han et al. studied the ZrPCN-222 carbonization with temperatures ranging from 600 to 900 °C and discovered that the ORR efficiency is correlated with the pyrolysis temperature (Figure 6A) [55]. The authors discovered the ORR efficiency thresholds at carbonization temperatures of about 700 °C, and particle downsizes up to 50 nm. Furthermore, HF etching shifts the ORR half-wave potential by 0.012 V, which is associated with the complete removal of inert ZrO_2 (Figure 6C,D), which increases the PC porosity (BET surface area increased from 437.8 to 594.2 m^2g^{-1}). At this carbonization temperature and particle sizes of about 320 nm, the ORR activity obtained for ZrPCN-222(Fe)/PC after HF etching had an $E_{1/2}$ = 0.87 V (versus RHE) in 0.1 M KOH and an $E_{1/2}$ = 0.79 V (versus RHE) in 0.1 M $HClO_4$. The n value of PCN was 4.0 (alkaline conditions) and 3.9 (under acidic conditions), indicating a 4e reduction process.

In the aforementioned examples, the final PC retains the morphology of the parent material, and little-to-no aggregation occurred to the metal centers. In some cases, adjacent metal ions with no protective layer between the MOF pores are usually prone to aggregate, forming inactive metal-based nanoparticles during the high-temperature calcination process. One workaround is to produce a stable PC with rich transition metal sub-nanometer clusters [56]. A recent work showed that this approach could provide an optimized electronic configuration to generate highly active ORR catalysts. This was possible by including Fe in ZrPCN-222 using a post-synthesis metalation methodology. Pyrolysis at 800 °C for 2 h in aN_2 atmosphere, followed by acid etching (HF, 5 wt% in water) for one day, yielded the corresponding Fe–FePC with an iron content around 0.93 wt%. This PC exhibited a superior electrocatalytic performance, with a positive onset potential of 0.95 V and a half-wave potential of 0.82 V in alkaline electrolyte (0.1 M KOH). These activities are comparable with commercial Pt/C (E_{onset} = 0.95 V, $E_{1/2}$ = 0.81 V). The Fe–FePC exhibited high stability with a cyclic voltammetry test for 5000 cycles, where a negative shift of 8 mV was observed for the half-wave potential.

This work showed the importance of the dispersion of iron cations on the final PC materials and demonstrated that it is imperative to develop simple and general approaches to prevent the aggregation of metal species to fabricate CP materials with active metal sites at an atomic level [57–59].

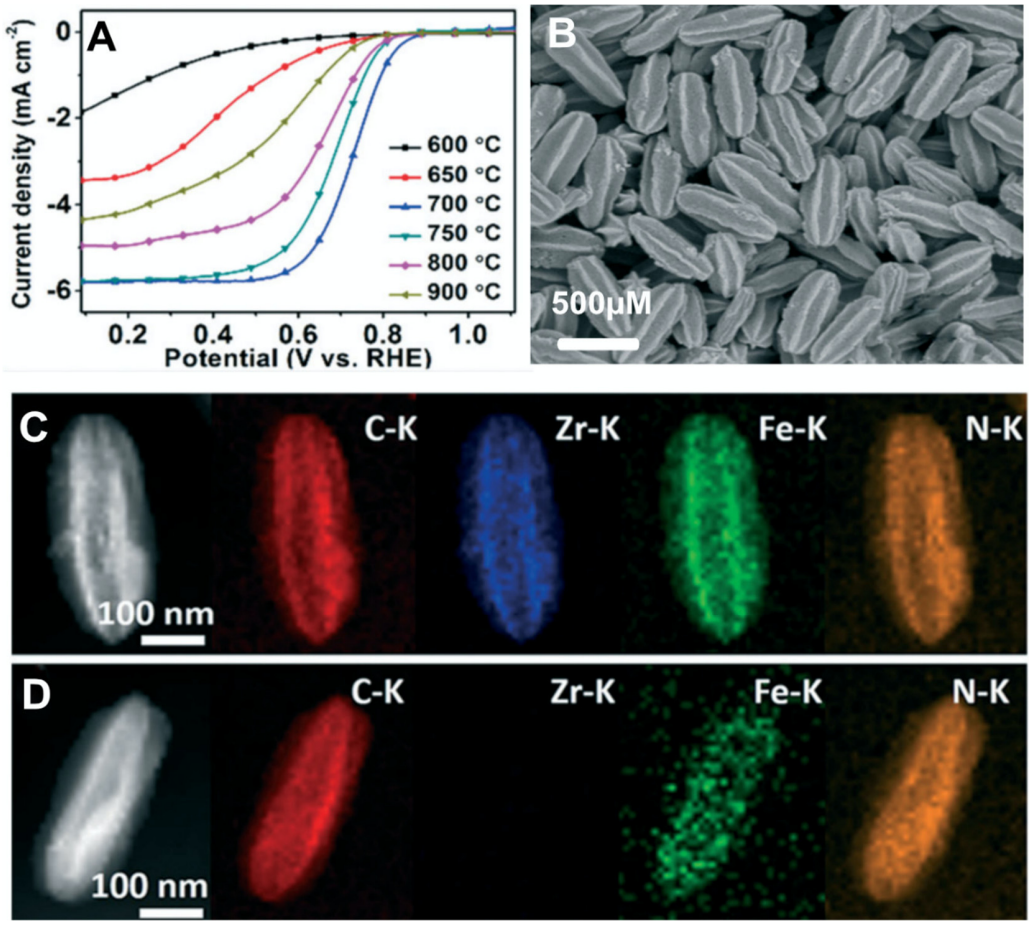

Figure 6. (**A**) ORR polarization curves affected by the pyrolysis temperature with nanocapsules at an average width of 320 nm (the electrocatalyst loaded onto RDE is 0.6 mg·cm^{-2}). (**B**) SEM image of ZrPCN-222(Fe)/PC before HF etching. (**C**) HAADF-STEM image of ZrPCN-222(Fe)/PC and the corresponding elemental mapping. (**D**) HAADF-STEM image of ZrPCN-222(Fe)/PC after HF etching and the corresponding elemental mapping. Reproduced with permission from [55]. Royal Society Chemistry, 2020.

2.2.1. Single Active Site MOF-Derived PC Materials

In order to achieve atomically dispersed metals in high loadings for efficient catalysis, Jiao et al. prepared ZrPCN-222 with a mixed-ligand strategy to afford a high-content (1.76 wt%) single-atom iron-implanted *N*-doped porous carbon (PC (Fe_{20})) by way of pyrolysis (Figure 7A) [57]. This was achieved by mixing Fe–TCPP with non-metallated TCPP with a molar ratio of 1:4 in the preparation of ZrMOF-222. The resulting MOF was carbonized at 800 °C for 2 h, and the remaining ZrO_2 was removed by immersing the sample in HF (20 wt%) for 6 h at 60 °C, achieving a BET surface area of 532 m^2g^{-1}. This Fe–N–PC material exhibited ORR activity with an $E_{1/2}$ = 0.89 V (versus RHE) in 0.1 M KOH and an $E_{1/2}$ = 0.78 V (versus RHE) in 0.1 M $HClO_4$. The periodic and tailorable MOF structure, with a spatial distance control of the iron centers in the porphyrinic core, suppressed iron aggregation during pyrolysis, leading to effective atomic dispersion in the final PC.

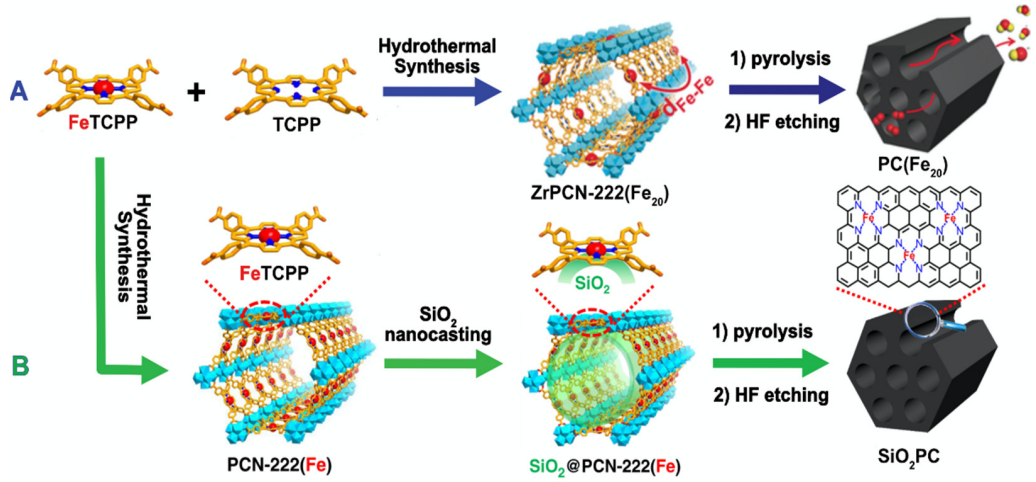

Figure 7. Schematic illustration showing: (**A**) the rational fabrication of the PC (Fe20) catalyst by way of a mixed-ligand strategy; (**B**) nano casting-assisted fabrication of single-atom Fe–N–C from the PCN-222 (Fe) MOF. Reproduced with permission from [57,59]. Wiley-VCH, 2018 and Nature, 2020.

More recently, the same research group included SiO_2 moieties into this porphyrin-based MOF system (ZrPCN-222(Fe)) to prevent iron migration and aggregation [59]. The high surface area (2040 $m^2\,g^{-1}$) and a pore size of 3.2 nm facilitated the inclusion of tetraethylorthosilicate (TEOS) into the PCN-222(Fe) mesopores (Figure 7B). Upon treatment with HCl vapor, the TEOS in ZrPCN-222(Fe) could be hydrolyzed and condensed to silica, affording a SiO_2@PCN-222(Fe) composite that retained the overall MOF crystallinity thanks to the high acidic stability of the ZrPCN-222MOF. The resulting material exhibited a much higher content in iron (3.46 wt%) than the previous report and improved ORR activity ($E_{1/2}$ = 0.90 V (versus RHE) in 0.1 M KOH and $E_{1/2}$ = 0.80 V (versus RHE) in 0.1 M $HClO_4$).

Using a similar strategy, Meng et al. incorporated polyaniline (PANI) into the pores of PCN-224 (Fe) followed by pyrolysis (at 900 °C) to obtain the single-atom Fe-implanted *N*-doped PC material PANI@PC [58]. PANI, inside the pores of PCN-224 (Fe), prevented the aggregation of the iron species during the thermal treatment, and acted as a nitrogen source to increase the nitrogen content and form Fe–N active sites. Compared with the ZrPCN-224 (Fe)-derived PC sample, carbonaceous PANI@PC showed higher nitrogen and iron contents (2.35 vs. 1.41 and 1.89 vs. 0.27 wt %, respectively). This comparison was reflected in the ORR performance showing that PANI@PC had an $E_{1/2}$ = 0.89 V (versus RHE) in 0.1 M KOH ($E_{1/2}$ = 0.82 V observed for PCN-224 PC) and an $E_{1/2}$ = 0.76 V (versus RHE) in 0.1 M $HClO_4$ ($E_{1/2}$ = 0.70 V observed for PCN-224 PC).

In general, with a higher (positive) half-wave potential and improved stability in both alkaline and acidic conditions, the migration-prevention strategy provides a useful tool to fabricate atomically dispersed metal active sites by way of pyrolysis to boost catalysis.

Ammonia (NH_3) is an activated nitrogen building block for modern fertilizers, plastics, fibers and explosives [60]. Its production is, however, limited to the traditional Haber–Bosch process. Very recently, the nitrogen electrocatalytic reduction reaction (NRR) has demonstrated to be a clean alternative, and sustainable approach to produce NH_3 and, for this reason, the system used for ORR illustrated in Figure 7A was recently re-used for an electrocatalytic nitrogen reduction reaction [61]. The concept was to understand if the NRR could benefit from the highly dispersed single-atom iron sites of PC (Fe_{20}). Interestingly, PC (Fe_{20}) showed a faradaic efficiency (FE) of 4.51% and an ammonia yield rate of 1.56×10^{-11} mol·cm^{-2}·s^{-1} at −0.05 V (versus RHE). These values were compared with the same PC materials bearing nickel and cobalt instead of iron centers, and proved to be superior. Nevertheless, as good as these values may be, they still require improvements mainly because the EF remains fairly low.

2.2.2. Bimetallic MOF-Derived PC Materials

As inferred from past research papers, the morphology of PC materials derived from porphyrin-based MOFs strongly relies on the type of precursor, dopant components, carbon support morphology and the post-treatment etching. There are not many examples in the literature where the PC materials are doped with active M–N_4 sites bearing a mixture of metal centers. Not only is this a difficult task, but it requires a stable porous MOF capable of enduring this process in a controlled fashion. In 2017, Fang et al. prepared a cubic-shaped ZrPCN-224 that was post-synthetically modified with iron and cobalt (with different ratios). Upon pyrolysis (900 °C) and a double acid etching treatment, PCN-224-(FeCo) was converted to *N*-doped PC nanocubes with a highly dispersed iron and cobalt content of 0.43 and 0.37 wt%, respectively (Figure 8) [62].

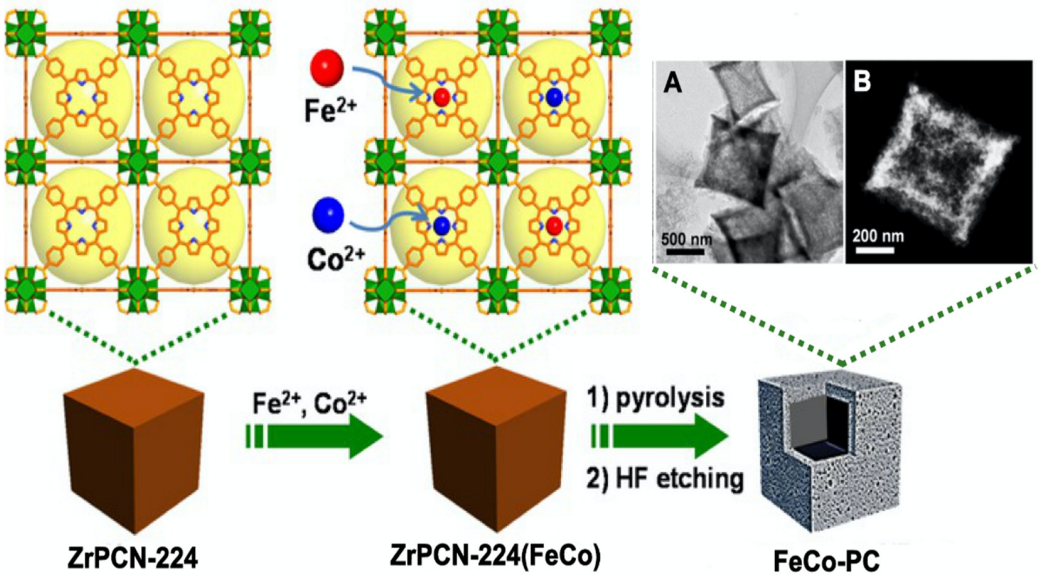

Figure 8. General preparation of (FeCo)PC: (**A**) TEM image of (FeCo)PC; (**B**) high-angle annular dark-field scanning TEM (HAADF-STEM). Reproduced with permission from [62]. Wiley-VCH, 2020.

The TEM studies showed a sharp contrast between the inner cavity and the outer carbon shell, indicating a hollow structure (Figure 8A,B). This morphology guarantees good accessibility of the active sites and efficient mass transfer. The PC inherited the cubic morphology and a similar crystal size of the parent ZrPCN-224(FeCo)MOF having a high BET surface area (1240 $m^2 \cdot g^{-1}$ vs. 2100 $m^2 \cdot g^{-1}$ of ZrPCN224(FeCo)) with approximately 3 nm pores. The co-existence of the Fe–N_4 and Co–N_4 species brought together active catalytic centers arising from both Fe and Co, ultimately contributing to the high graphitic level of the carbon network and enhanced corrosion resistance. These structural features synergistically boost the ORR activity and, as a result, the optimized (FeCo)PC composite exhibits superior electrocatalytic ORR performance both in alkaline and acidic solutions (E_{onset} = 0.97 V and an $E_{1/2}$ = 0.87 V (versus RHE) in 0.1 M KOH and E_{onset} = 0.85 V and $E_{1/2}$ = 0.74 V (versus RHE) in 0.1 m $HClO_4$).

Nickel has found its way into porous carbons for application in ORR combined in a PC matrix alongside with iron [63]. The ZrPCN-221 was prepared by hydrothermal synthesis with a mixture of Ni porphyrins and Fe porphyrins in a ratio of 9:1 [63]. This approach proved less versatile than the post-metalation methodology described by Fang et al. because higher amounts of iron porphyrin (changing the ratio to 8:2) led to the formation of stacking bulks, and the crystal structure of the product presented a mixture of ZrPCN-221 and ZrPCN-222 [62]. Subsequent pyrolysis (800 °C, N_2 atmosphere for 3 h) and acid etching (HF) of ZrPCN-221(NiFe) produced a PC material with an *N*-doped hierarchical graphitic carbon with Ni and Fe contents of 1.65% and 0.13%, respectively. The PC catalyst showed high ORR activity and stability with a large diffusion-limited

current density (6.19 mA·cm^{-2}) and a half-wave potential of 0.83 V (vs. RHE). Systematic experiments and structural characterization revealed that the favorable internal space and unique hierarchical structure with numerous nitrogen-doped Ni–N_4 sites synergistically contribute to the enhanced catalytic activity compared with the commercial Pt/C catalyst ($E_{1/2}$ = 0.82 V and j_L, 5.57 mA·cm^{-2}). Furthermore, the electron transfer number was calculated to be approximately four from 0.45 to 0.6 V, being stable for up to 10,000 cycles. The use of two metals inside the core has showed that bimetallic PC carbons can provide interesting results as electrocatalysts.

With a different approach, Fang et al. prepared a PC composite material bearing iron oxide and nickel centers, growing FePCN-600(Ni) on graphene oxide [64]. Upon pyrolysis and phosphidation with NaH_2PO_2, the FePCN600(Ni)/GO composite was transformed into a sheet-like FeNi−P/rGO PC.

The integration of Fe and Ni elements, with the highly porous features of PCN-600, and the enhanced conductivity of GO, makes the optimized FeNi−P/rGO PC composite exhibit a high oxygen evolution reaction (OER) catalytic performance, ultimately achieving a current density of 10 mA·cm^{-2} at an overpotential as low as 240 mV. Interestingly, this value surpasses the state-of-the-art IrO_2 and puts this PC composite amongst the most active OER catalysts reported to date (overpotential at 400 mV).

Concerning the materials preparation, this methodology can present some advantages when compared with the previous methods, where challenges associated with the formation of phase mixtures were observed (when trying to use mixtures of metallated porphyrins), and the difficult control of the amounts and ratios of metals included in the MOF network in the post-synthesis method can hinder further developments of multiple metal MOF-derived PCs.

In general, the applications where MOF-derived porous carbons are mostly used are related with electrochemical reactions. In the next table (Table 1), this trend is resumed with the most important characteristics of the PC prepared from porphyrin MOFs.

Table 1. Electrochemical characteristics of the PC materials prepared from porphyrin MOFs.

MOF	Carbonization Temperature (Atmosphere, Time)	$S_{(BET)}$ (m^2g^{-1})	Catalytic Activity			Ref
			Nitrophenol Reduction			
			Activation Energy (kJ·mol^{-1})	Pseudo-First-Order Kinetics (s^{-1})		
ZrPCN-224	700 °C (N_2, 1 h)	1089	26.4	5.3×10^{-3}		[48]
			Electrochemical Capacitor			
			Current density (Ag^{-1})	Capacitance ($F{\cdot}g^{-1}$)	Electrolyte	
ZrMOF-525	800 °C (N_2, 1 h)	786	2	425	1 M H_2SO_4	[49]
			Carbon Dioxide Electroreduction			
			Faradaic Efficiency (%)	Potential (vs. RHE)	Electrolyte	
ZrPCN-222	800 °C (N_2, 2 h)	37	13	−1.0	0.5 M $KHCO_3$	[50]
ZrPCN-224	1000 °C (N_2, 2 h)	289	14	−0.8	0.5 M $KHCO_3$	
			Oxygen Reduction Reaction (ORR)			
			$E_{1/2}$ (V vs. RHE)	Electron transfer number (electrons)	electrolyte	
ZrCPM-99(Fe)	700 °C (N_2, 2 h)	*399*	0.80	4	0.1 M KOH	[51]
			0.87	4	0.1 M $HClO_4$	
ZrPCN-222(Cu)	900 °C (N_2 and 1% Air, 2 h)	240		4	0.1 M KOH	[52]
ZrPCN-222(Fe)	700 °C (Ar, 2 h)	594	0.87		0.1 M KOH	[55]
			0.79		0.1 M $HClO_4$	
	800 °C (N_2, 2 h)	433	0.82	4	0.1 M KOH	[56]
	800 °C (N_2, 2 h)	532	0.89	4	0.1 M KOH	[57]
			0.78	4	0.1 M $HClO_4$	
	800 °C (N_2, 2 h)	1615	0.90	4	0.1 M KOH	[59]
			0.80	4	0.1 M $HClO_4$	

Table 1. *Cont.*

MOF	Carbonization Temperature (Atmosphere, Time)	$S_{(BET)}$ (m^2g^{-1})	Catalytic Activity			Ref
			Nitrophenol Reduction			
			Activation Energy ($kJ \cdot mol^{-1}$)	Pseudo-First-Order Kinetics (s^{-1})		
ZrPCN-224(Fe)	800 °C (Ar, 1 h)	554	0.87 0.76	4 4	0.1 M KOH 0.1 M $HClO_4$	[54]
	900 °C (N_2, 2 h)	430	0.89 0.76	4 4	0.1 M KOH 0.1 M $HClO_4$	[58]
ZrPCN-224 (FeCo)	900 °C (N_2, 2 h)		0.87 0.74	4 4	0.1 M KOH 0.1 M $HClO_4$	[62]
ZrPCN-221(NiFe)	800 °C (N_2, 3 h)	557	0.83	4	0.1 M KOH	[63]
			Nitrogen Reduction Reaction (NRR)			
			Faradaic Efficiency (%)	Ammonia yield Rate (−0.05 V vs. RHE $mol \cdot cm^{-2} \cdot s^{-1}$)		
ZrPCN-222(Fe)	800 °C (N_2, 2 h)	1615	4.51	1.56×10^{-11}		[61]
			Oxygen Evolution Reaction (OER)			
			Current Density ($mA \cdot cm^{-2}$)	Overpotential (mV)		
FePCN-600(Ni)	700 °C (N_2, 2 h)	59	10	240		[64]

3. Conclusions

The research on MOF-derived nitrogen-doped porous carbon electrocatalysts achieved significant signs of development in recent years, with most of the studies herein reviewed being published in the last five years (or so). Despite some remarkable advancements, a great number of challenges still have to be surpassed before these materials achieve enough maturity for real application in electrocatalysis.

Currently, the development of highly efficient non-precious metal catalysts to replace Pt-based ones (or other precious ones) under acidic conditions remains a great challenge, requiring several efforts to modify MOF precursors to a given application in electrocatalysis. There are a vast number of parameters to control, and more studies need to be taken into account before real structure-affinity conclusions can be made on the PC materials here described derived from porphyrin-based MOFs. For this particular family of PCs, it is believed that metal doping can form the M–N_4 bonds, which are in general favorable for electrocatalysts. Nonetheless, the role of the metal active site is not yet clearly understood, and the structure affinity incurred by doping other metal centers into the porous carbons are still challenging.

We further emphasize that not many studies were performed with non-metal porphyrin MOFs. Moreover, studies with other non-metal doping sources (e.g., phosphorus, sulfur, boron, and fluorine) remain inexistent.

This review shows that a correct choice of the initial MOF precursor and of its morphology can play a decisive role in the obtained PC materials, with several retaining the same morphology and pore structure of the parent MOFs. Furthermore, some of these studies can allow control of the metal sites in the PC materials at an atomic scale, effectively providing insights on the role of the metal sites in these networks. These are, undeniably, significant advancements towards the development of highly efficient PC electrocatalysts from porphyrin-based MOFs.

A handful of reports in the literature described the effect of different porphyrin MOF backbones in the preparation of functional PCs. Despite their potential, there is still much to learn about these materials and how properties such as crystal morphology, size, and dispersion affect their performance.

In short, PCs obtained from porphyrin-based MOF remain a largely underexplored research field. Further investigations will likely reveal new parameters and novel applications for these materials that may prosper in some areas in the next few years.

Author Contributions: Conceptualization, research and writing—review and editing, F.F.; proof-reading and funding acquisition, F.A.A.P. All authors have read and agreed to the published version of the manuscript.

Funding: This research was funded by FCT, grant numbers UIDB/50011/2020 and UIDP/50011/2020. The research contract of FF (REF-168-89-ARH/2018) is funded by national funds (OE), through FCT, in the scope of the framework contract foreseen in nos. 4, 5 and 6 of article 23 of the Decree-Law 57/2016, of 29 August, changed by Law 57/2017, of 19 July.

Institutional Review Board Statement: Not applicable.

Acknowledgments: This work was developed within the scope of the project CICECO—Aveiro Institute of Materials (UIDB/50011/2020 and UIDP/50011/2020) research unit, financed by national funds through the FCT/MEC and when appropriate co-financed by FEDER under the PT2020. The research contract of FF (REF-168-89-ARH/2018) is funded by national funds (OE), through FCT, in the scope of the framework contract foreseen in Nos. 4, 5 and 6 of article 23 of the Decree-Law 57/2016, of 29 August, changed by Law 57/2017, of 19 July.

Conflicts of Interest: The authors declare no conflict of interest.

References

1. Yuan, S.; Feng, L.; Wang, K.; Pang, J.; Bosch, M.; Lollar, C.; Sun, Y.; Qin, J.; Yang, X.; Zhang, P.; et al. Stable Metal–Organic Frameworks: Design, Synthesis, and Applications. *Adv. Mater.* **2018**, *30*, 1704303. [CrossRef]
2. Kumar, S.; Jain, S.; Nehra, M.; Dilbaghi, N.; Marrazza, G.; Kim, K.-H. Green synthesis of metal–organic frameworks: A state-of-the-art review of potential environmental and medical applications. *Coord. Chem. Rev.* **2020**, *420*, 213407. [CrossRef]
3. Wang, P.-L.; Xie, L.-H.; Joseph, E.A.; Li, J.-R.; Su, X.-O.; Zhou, H.-C. Metal–Organic Frameworks for Food Safety. *Chem. Rev.* **2019**, *119*, 10638–10690. [CrossRef]
4. Mendes, R.F.; Figueira, F.; Leite, J.P.; Gales, L.; Almeida Paz, F.A. Metal–organic frameworks: A future toolbox for biomedicine? *Chem. Soc. Rev.* **2020**, *49*, 9121–9153. [CrossRef]
5. Pascanu, V.; González Miera, G.; Inge, A.K.; Martín-Matute, B. Metal–Organic Frameworks as Catalysts for Organic Synthesis: A Critical Perspective. *J. Am. Chem. Soc.* **2019**, *141*, 7223–7234. [CrossRef] [PubMed]
6. Wen, M.; Li, G.; Liu, H.; Chen, J.; An, T.; Yamashita, H. Metal–organic framework-based nanomaterials for adsorption and photocatalytic degradation of gaseous pollutants: Recent progress and challenges. *Environ. Sci. Nano* **2019**, *6*, 1006–1025. [CrossRef]
7. Li, H.; Wang, K.; Sun, Y.; Lollar, C.T.; Li, J.; Zhou, H.-C. Recent advances in gas storage and separation using metal–organic frameworks. *Mater. Today* **2018**, *21*, 108–121. [CrossRef]
8. Figueira, F.S.; Barbosa, J.F.; Mendes, R.S.; Braga, S.A. Almeida Paz, F. Virus meet metal-organic frameworks: A nanoporous solution to a world-sized problem? *Mater. Today* **2020**. [CrossRef]
9. Mohanty, A.; Jaihindh, D.; Fu, Y.-P.; Senanayak, S.P.; Mende, L.S.; Ramadoss, A. An extensive review on three dimension architectural Metal-Organic Frameworks towards supercapacitor application. *J. Power Sources* **2021**, *488*, 229444. [CrossRef]
10. Aguilera-Sigalat, J.; Bradshaw, D. Synthesis and applications of metal-organic framework–quantum dot (QD@MOF) composites. *Coord. Chem. Rev.* **2016**, *307*, 267–291. [CrossRef]
11. Xue, Y.; Zheng, S.; Xue, H.; Pang, H. Metal–organic framework composites and their electrochemical applications. *J. Mater. Chem. A* **2019**, *7*, 7301–7327. [CrossRef]
12. Liu, W.; Yin, X.-B. Metal–organic frameworks for electrochemical applications. *TrAC Trends Anal. Chem.* **2016**, *75*, 86–96. [CrossRef]
13. Morozan, A.; Jaouen, F. Metal organic frameworks for electrochemical applications. *Energy Environ. Sci.* **2012**, *5*, 9269–9290. [CrossRef]
14. Cai, Z.-X.; Wang, Z.-L.; Kim, J.; Yamauchi, Y. Hollow Functional Materials Derived from Metal–Organic Frameworks: Synthetic Strategies, Conversion Mechanisms, and Electrochemical Applications. *Adv. Mater.* **2019**, *31*, 1804903. [CrossRef]
15. Zhao, Z.; Ding, J.; Zhu, R.; Pang, H. The synthesis and electrochemical applications of core–shell MOFs and their derivatives. *J. Mater. Chem. A* **2019**, *7*, 15519–15540. [CrossRef]
16. Xiao, X.; Zou, L.; Pang, H.; Xu, Q. Synthesis of micro/nanoscaled metal–organic frameworks and their direct electrochemical applications. *Chem. Soc. Rev.* **2020**, *49*, 301–331. [CrossRef]
17. Yi, F.-Y.; Zhang, R.; Wang, H.; Chen, L.-F.; Han, L.; Jiang, H.-L.; Xu, Q. Metal–Organic Frameworks and Their Composites: Synthesis and Electrochemical Applications. *Small Methods* **2017**, *1*, 1700187. [CrossRef]
18. Tajik, S.; Beitollahi, H.; Nejad, F.G.; Kirlikovali, K.O.; Van Le, Q.; Jang, H.W.; Varma, R.S.; Farha, O.K.; Shokouhimehr, M. Recent Electrochemical Applications of Metal–Organic Framework-Based Materials. *Cryst. Growth Des.* **2020**, *20*, 7034–7064. [CrossRef]
19. Calbo, J.; Golomb, M.J.; Walsh, A. Redox-active metal–organic frameworks for energy conversion and storage. *J. Mater. Chem. A* **2019**, *7*, 16571–16597. [CrossRef]

20. D'Alessandro, D.M. Exploiting redox activity in metal–organic frameworks: Concepts, trends and perspectives. *Chem. Commun.* **2016**, *52*, 8957–8971. [CrossRef]
21. Zha, Q.; Rui, X.; Wei, T.; Xie, Y. Recent advances in the design strategies for porphyrin-based coordination polymers. *CrystEngComm* **2014**, *16*, 7371–7384. [CrossRef]
22. Scandola, F.; Chiorboli, C.; Prodi, A.; Iengo, E.; Alessio, E. Photophysical properties of metal-mediated assemblies of porphyrins. *Coord. Chem. Rev.* **2006**, *250*, 1471–1496. [CrossRef]
23. Figueira, F.M.R.; Pereira, P.; Silva, S.A.S.; Cavaleiro, J.P.C.; Tome, J. Porphyrins and Phthalocyanines Decorated with Dendrimers: Synthesis and Biomedical Applications. *Curr. Org. Synth.* **2014**, *11*, 110–126. [CrossRef]
24. Figueira, F.; Cavaleiro, J.A.S.; Tomé, J.P.C. Silica nanoparticles functionalized with porphyrins and analogs for biomedical studies. *J. Porphyr. Phthalocyanines* **2011**, *15*, 517–533. [CrossRef]
25. Figueira, F.; Rodrigues, J.M.M.; Farinha, A.A.S.; Cavaleiro, J.A.S.; Tomé, J.P.C. Synthesis and anion binding properties of porphyrins and related compounds. *J. Porphyr. Phthalocyanines* **2016**, *20*, 950–965. [CrossRef]
26. Singh, S.; Aggarwal, A.; Bhupathiraju, N.V.S.D.K.; Arianna, G.; Tiwari, K.; Drain, C.M. Glycosylated Porphyrins, Phthalocyanines, and Other Porphyrinoids for Diagnostics and Therapeutics. *Chem. Rev.* **2015**, *115*, 10261–10306. [CrossRef]
27. Hiroto, S.; Miyake, Y.; Shinokubo, H. Synthesis and Functionalization of Porphyrins through Organometallic Methodologies. *Chem. Rev.* **2017**, *117*, 2910–3043. [CrossRef]
28. Auwärter, W.; Écija, D.; Klappenberger, F.; Barth, J.V. Porphyrins at interfaces. *Nat. Chem.* **2015**, *7*, 105–120. [CrossRef]
29. Liang, Z.; Wang, H.-Y.; Zheng, H.; Zhang, W.; Cao, R. Porphyrin-based frameworks for oxygen electrocatalysis and catalytic reduction of carbon dioxide. *Chem. Soc. Rev.* **2021**, *50*, 2540–2581. [CrossRef]
30. Zheng, F.; Zhang, Z.; Zhang, C.; Chen, W. Advanced Electrocatalysts Based on Metal–Organic Frameworks. *ACS Omega* **2020**, *5*, 2495–2502. [CrossRef]
31. Xiao, Y.-H.; Gu, Z.-G.; Zhang, J. Surface-coordinated metal–organic framework thin films (SURMOFs) for electrocatalytic applications. *Nanoscale* **2020**, *12*, 12712–12730. [CrossRef]
32. Kitagawa, S.; Noro, S.-I.; Nakamura, T. Pore surface engineering of microporous coordination polymers. *Chem. Commun.* **2006**, 701–707. [CrossRef]
33. Wang, H.; Zhu, Q.-L.; Zou, R.; Xu, Q. Metal-Organic Frameworks for Energy Applications. *Chem* **2017**, *2*, 52–80. [CrossRef]
34. Baumann, A.E.; Burns, D.A.; Liu, B.; Thoi, V.S. Metal-organic framework functionalization and design strategies for advanced electrochemical energy storage devices. *Commun. Chem.* **2019**, *2*, 86. [CrossRef]
35. Castro, K.A.D.F.; Figueira, F.; Almeida Paz, F.A.; Tomé, J.P.C.; da Silva, R.S.; Nakagaki, S.; Neves, M.G.P.M.S.; Cavaleiro, J.A.S.; Simões, M.M.Q. Copper-phthalocyanine coordination polymer as a reusable catechol oxidase biomimetic catalyst. *Dalton Trans.* **2019**, *48*, 8144–8152. [CrossRef]
36. Pereira, C.F.; Liu, Y.; Howarth, A.; Figueira, F.; Rocha, J.; Hupp, J.T.; Farha, O.K.; Tomé, J.P.C.; Almeida Paz, F.A. Detoxification of a Mustard-Gas Simulant by Nanosized Porphyrin-Based Metal–Organic Frameworks. *ACS Appl. Nano Mater.* **2019**, *2*, 465–469. [CrossRef]
37. Pereira, C.F.; Figueira, F.; Mendes, R.F.; Rocha, J.; Hupp, J.T.; Farha, O.K.; Simões, M.M.Q.; Tomé, J.P.C.; Paz, F.A.A. Bifunctional Porphyrin-Based Nano-Metal–Organic Frameworks: Catalytic and Chemosensing Studies. *Inorg. Chem.* **2018**, *57*, 3855–3864. [CrossRef] [PubMed]
38. Chen, J.; Zhu, Y.; Kaskel, S. Porphyrin-Based Metal–Organic Frameworks for Biomedical Applications. *Angew. Chem. Int. Ed.* **2021**, *60*, 5010–5035. [CrossRef]
39. Carrasco, S. Metal-Organic Frameworks for the Development of Biosensors: A Current Overview. *Biosensors* **2018**, *8*, 92. [CrossRef] [PubMed]
40. Xu, Y.; Li, Q.; Xue, H.; Pang, H. Metal-organic frameworks for direct electrochemical applications. *Coord. Chem. Rev.* **2018**, *376*, 292–318. [CrossRef]
41. Yu, F.; Bai, X.; Liang, M.; Ma, J. Recent progress on metal-organic framework-derived porous carbon and its composite for pollutant adsorption from liquid phase. *Chem. Eng. J.* **2021**, *405*, 126960. [CrossRef]
42. Chen, L.; Wang, H.-F.; Li, C.; Xu, Q. Bimetallic metal–organic frameworks and their derivatives. *Chem. Sci.* **2020**, *11*, 5369–5403. [CrossRef]
43. Yang, L.; Zeng, X.; Wang, W.; Cao, D. Recent Progress in MOF-Derived, Heteroatom-Doped Porous Carbons as Highly Efficient Electrocatalysts for Oxygen Reduction Reaction in Fuel Cells. *Adv. Funct. Mater.* **2018**, *28*, 1704537. [CrossRef]
44. Peh, S.B.; Wang, Y.; Zhao, D. Scalable and Sustainable Synthesis of Advanced Porous Materials. *ACS Sustain. Chem. Eng.* **2019**, *7*, 3647–3670. [CrossRef]
45. Zhang, X.; Wasson, M.C.; Shayan, M.; Berdichevsky, E.K.; Ricardo-Noordberg, J.; Singh, Z.; Papazyan, E.K.; Castro, A.J.; Marino, P.; Ajoyan, Z.; et al. A historical perspective on porphyrin-based metal–organic frameworks and their applications. *Coord. Chem. Rev.* **2021**, *429*, 213615. [CrossRef] [PubMed]
46. Song, Z.; Zhang, L.; Doyle-Davis, K.; Fu, X.; Luo, J.-L.; Sun, X. Recent Advances in MOF-Derived Single Atom Catalysts for Electrochemical Applications. *Adv. Energy Mater.* **2020**, *10*, 2001561. [CrossRef]
47. Osmieri, L. Transition Metal–Nitrogen–Carbon (M–N–C) Catalysts for Oxygen Reduction Reaction. Insights on Synthesis and Performance in Polymer Electrolyte Fuel Cells. *ChemEngineering* **2019**, *3*, 16. [CrossRef]

48. Huang, G.; Yang, L.; Ma, X.; Jiang, J.; Yu, S.-H.; Jiang, H.-L. Metal–Organic Framework-Templated Porous Carbon for Highly Efficient Catalysis: The Critical Role of Pyrrolic Nitrogen Species. *Chem. Eur. J.* **2016**, *22*, 3470–3477. [CrossRef]
49. Chang, T.-H.; Young, C.; Lee, M.-H.; Salunkhe, R.R.; Alshehri, S.M.; Ahamad, T.; Islam, M.T.; Wu, K.C.W.; Hossain, M.S.A.; Yamauchi, Y.; et al. Synthesis of MOF-525 Derived Nanoporous Carbons with Different Particle Sizes for Supercapacitor Application. *Chem. Asian J.* **2017**, *12*, 2857–2862. [CrossRef]
50. Hou, Y.; Hu, X.-J.; Tong, H.-Y.; Huang, Y.-B.; Cao, R. Unraveling the relationship of the pore structures between the metal-organic frameworks and their derived carbon materials. *Inorg. Chem. Commun.* **2020**, *114*, 107825. [CrossRef]
51. Lin, Q.; Bu, X.; Kong, A.; Mao, C.; Zhao, X.; Bu, F.; Feng, P. New Heterometallic Zirconium Metalloporphyrin Frameworks and Their Heteroatom-Activated High-Surface-Area Carbon Derivatives. *J. Am. Chem. Soc.* **2015**, *137*, 2235–2238. [CrossRef] [PubMed]
52. Volosskiy, B.; Fei, H.; Zhao, Z.; Lee, S.; Li, M.; Lin, Z.; Papandrea, B.; Wang, C.; Huang, Y.; Duan, X. Tuning the Catalytic Activity of a Metal–Organic Framework Derived Copper and Nitrogen Co-Doped Carbon Composite for Oxygen Reduction Reaction. *ACS Appl. Mater. Interfaces* **2016**, *8*, 26769–26774. [CrossRef]
53. Mei, H.-M.; Li, S.; Dong, J.-R.; Zhang, L.; Su, C.-Y. Porphyrinic Metal-Organic Frameworks Derived Carbon-Based Nanomaterials for Hydrogen Evolution Reaction. *ChemistrySelect* **2020**, *5*, 10988–10995. [CrossRef]
54. Hua, X.; Luo, J.; Shen, C.; Chen, S. Hierarchically porous Fe–N–C nanospindles derived from a porphyrinic coordination network for oxygen reduction reaction. *Catal. Sci. Technol.* **2018**, *8*, 1945–1952. [CrossRef]
55. Han, H.; Zhang, Y.; Cong, Y.; Qin, J.; Zhai, Z.; Wang, X.; Gao, R.; Zhang, G.; Guo, X.; Song, Y. Pyrolysis-driven synthesis of nanoscale carambola-like carbon decorated with atomically dispersed Fe sites toward efficient oxygen reduction reaction. *Catal. Sci. Technol.* **2020**, *10*, 7160–7164. [CrossRef]
56. Wu, X.; Dong, J.; Qiu, M.; Li, Y.; Zhang, Y.; Zhang, H.; Zhang, J. Subnanometer iron clusters confined in a porous carbon matrix for highly efficient zinc–air batteries. *Nanoscale Horizons* **2020**, *5*, 359–365. [CrossRef]
57. Jiao, L.; Wan, G.; Zhang, R.; Zhou, H.; Yu, S.-H.; Jiang, H.-L. From Metal–Organic Frameworks to Single-Atom Fe Implanted N-doped Porous Carbons: Efficient Oxygen Reduction in Both Alkaline and Acidic Media. *Angew. Chem. Int. Ed.* **2018**, *57*, 8525–8529. [CrossRef]
58. Meng, D.-L.; Chen, C.-H.; Yi, J.-D.; Wu, Q.; Liang, J.; Huang, Y.-B.; Cao, R. Migration-Prevention Strategy to Fabricate Single-Atom Fe Implanted N-Doped Porous Carbons for Efficient Oxygen Reduction. *Research* **2019**, *2019*, 1768595. [CrossRef]
59. Jiao, L.; Zhang, R.; Wan, G.; Yang, W.; Wan, X.; Zhou, H.; Shui, J.; Yu, S.-H.; Jiang, H.-L. Nanocasting SiO_2 into metal–organic frameworks imparts dual protection to high-loading Fe single-atom electrocatalysts. *Nat. Commun.* **2020**, *11*, 2831. [CrossRef]
60. Guo, X.; Du, H.; Qu, F.; Li, J. Recent progress in electrocatalytic nitrogen reduction. *J. Mater. Chem. A* **2019**, *7*, 3531–3543. [CrossRef]
61. Zhang, R.; Jiao, L.; Yang, W.; Wan, G.; Jiang, H.-L. Single-atom catalysts templated by metal–organic frameworks for electrochemical nitrogen reduction. *J. Mater. Chem. A* **2019**, *7*, 26371–26377. [CrossRef]
62. Fang, X.; Jiao, L.; Yu, S.-H.; Jiang, H.-L. Metal–Organic Framework-Derived FeCo-N-Doped Hollow Porous Carbon Nanocubes for Electrocatalysis in Acidic and Alkaline Media. *ChemSusChem* **2017**, *10*, 3019–3024. [CrossRef] [PubMed]
63. He, T.; Ni, B.; Ou, Y.; Lin, H.; Zhang, S.; Li, C.; Zhuang, J.; Hu, W.; Wang, X. Nanosheet-Assembled Hierarchical Carbon Nanoframeworks Bearing a Multiactive Center for Oxygen Reduction Reaction. *Small Methods* **2018**, *2*, 1800068. [CrossRef]
64. Fang, X.; Jiao, L.; Zhang, R.; Jiang, H.-L. Porphyrinic Metal–Organic Framework-Templated Fe–Ni–P/Reduced Graphene Oxide for Efficient Electrocatalytic Oxygen Evolution. *ACS Appl. Mater. Interfaces* **2017**, *9*, 23852–23858. [CrossRef] [PubMed]